Title: RNA Polymerase II-mediated transcription is required for repair of ribosomal DNA breaks in nucleolar caps, guarding against genomic instability

- **Short Title: RNAPII promotes ribosomal DNA stability**

Authors

Cintia Checa-Rodríguez[1,2], Beatriz Suárez-Quintero[1,2], Laura Contreras[1,2], Lea Korsholm[3,$], Dorthe Helena Payne-Larsen[3], Jesús de la Cruz[1,2], Jiri Bartek[4,5], Daniel Gómez-Cabello[1,2,6*].

Affiliations

1. Instituto de Biomedicina de Sevilla (IBiS), Hospital Universitario Virgen del Rocío/CSIC/Universidad de Sevilla, 41013 Seville, Spain.

2. Departamento de Genética, Facultad de Biología, Universidad de Sevilla, 41012 Seville, Spain.

3. Nucleolar Stress and Disease Group, Danish Cancer Society Research Center, Strandboulevarden 49, Copenhagen, DK-2100, Denmark.

4. Genome Integrity Group, Danish Cancer Society Research Center, Strandboulevarden 49, Copenhagen, DK-2100, Denmark.

5. Division of Genome Biology, Department of Medical Biochemistry and Biophysics, Science for Life Laboratory, Karolinska Institute, Scheele's vag 2, Stockholm, 17177, Sweden.

6. Departamento de Biología Celular, Facultad de Biología, Universidad de Sevilla, 41012 Seville, Spain.

$. Present address: Center for Genomic Medicine, Rigshospitalet, Copenhagen University Hospital, Copenhagen, Denmark.

*Corresponding author. Email: dgcabello@us.es

Abstract (max 200 words)

Oversized nucleoli and enhanced ribosome biogenesis are hallmarks of cancer, reflecting tumor cells' aberrantly high demand for protein synthesis during tumorigenesis. The high-copy ribosomal DNA (rDNA) genes are highly transcribed by RNA Polimerase I (RNAPI) and inherently unstable, often subject to DNA double-strand breaks (DSBs) caused by transcription-replication conflicts. When DSBs happen, RNAPI becomes silenced by ATM signaling and rDNA DSBs are translocated to nucleolar periphery for repair mainly by homologous recombination in newly formed nucleolar caps. The molecular mechanisms underlying these processes are incompletely understood. Herein, we report that rDNA DSB translocation and nucleolar cap formation require the presence and activity of RNAPII. Nascent RNA deficiency upon RNAPII inhibition in rDNA damaged cells provoke rDNA instability and cell death. Finally, the enhanced cytotoxic effect of combined RNA transcription inhibition and rDNA damage, reported here, is consistent with addiction of cancer to nucleolar function, indicating an emerging targetable vulnerability of cancer cells that may inspire innovative treatment strategies in oncology.

Teaser (one sentence, max125 char./= short abstract)

Nascent RNA synthesis by RNA PolymeraseII safeguards ribosomal DNA integrity to avoid genomic instability in human cells.

Graphical Abstract

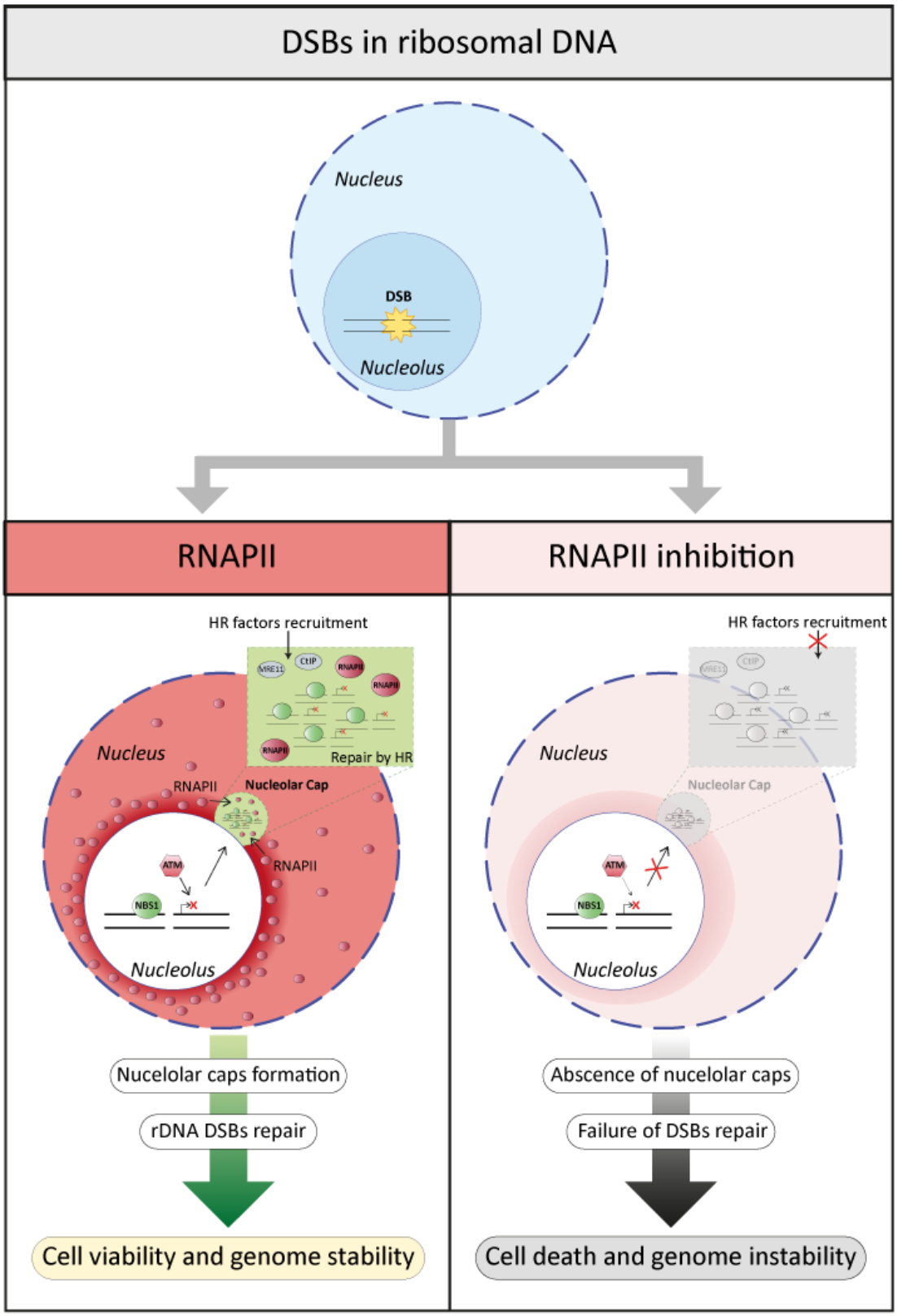

MAIN TEXT

Introduction

The nucleolus is a cellular sensor for diverse exogenous and intracellular insults. The nucleolus is a membrane-less intranuclear organelle whose canonical function is ribosome biogenesis (RiBi). RiBi includes a high ribosomal DNA (rDNA) transcription rate, rRNA processing and assembly of ribosomal subunits that are orchestrated in a complex multistep process leading to ribosome formation (1). Enlarged nucleoli due to elevated protein synthesis and cell metabolism, including RiBi, adapted to cope with aberrant growth and proliferation, is one of the long-established hallmarks of cancer cells (2). The nucleolus is also considered a central response hub for the stressors that promote cancer development (3). The study of nucleolar stress has been motivated, among other reasons, by efforts to interfere with RiBi function or inhibit RNA polymerase I (RNAPI), the enzyme responsible for rDNA genes, as strategies for cancer treatment in both preclinical and clinical settings (4,5).

The human genome contains around 200-600 tandem repeats of rDNA genes dispersed in chromosomes 13, 14, 15, 21 and 22. The active rDNA sequences are concentrated in the nucleolar organizer regions (NORs), which are prone to generate replication-transcription conflicts potentially leading to genome instability (6). Such conflicts occur because RNAPI-mediated transcription represents almost 60% of the total cellular transcription in eukaryotic cells (7). The occurrence of such hazardous transcription-replication conflicts is enhanced in tumor cells which show both aberrantly elevated rDNA transcription and deregulated genome replication as common features of oncogenic transformation. Due to such 'nucleolar stress', rDNA instability occurs commonly during tumorigenesis, likely fueling tumor progression due to rDNA rearrangements events including insertions, translocations and amplifications (8). Among the different rDNA damage arising from transcription-replication conflicts, the rDNA double-strand breaks (rDNA DSBs) are arguably the most cytotoxic and difficult to repair lesions (9-11). The two main pathways for DSB repair are homologous recombination (HR) and non-homologous end joining (NHEJ), both of which contribute to rDNA stability upon oncogenic or genotoxic stresses, such as activated cMYC oncogene and ionizing radiation (IR), respectively (11,12). The NHEJ process involves little if any DNA end processing and is potentially mutagenic. On the other hand, the HR pathway is a more precise DSB repair mechanism that avoids loss of genetic information, due to faithful repair based on using a homologous DNA sequence as a template (10,13). However, the HR machinery is largely absent from the nucleolar interior since intra-nucleolar recombination processes would induce illegitimate rearrangements among the many rDNA repeats localized on different chromosomes, with surely catastrophic consequences for the cell (14).

The complex spatio-temporal distribution of the DNA damage signaling and repair factors in response to rDNA lesions remains incompletely understood. Recently, it has shown that upon rDNA DSB formation, ATM-TCOF axis activation promotes transient transcriptional inhibition of RNAPI and rDNA relocalisation into newly formed structures at the nucleolar periphery, known as nucleolar caps (15-17). However, the roles of various HR factors in rDNA damage repair appear to be controversial, depending on the type of the DSB-inducing insult, for example, IR *versus* the enzymatically induced DNA breaks (18). Moreover, it has not yet been established what is the precise mechanism behind the observed relocation of some rDNA DSBs to the nucleolar periphery for their HR-mediated repair.

Recently, we and others have demonstrated the essential role of RNAPII and RNA polymerase III (RNAPIII) in the cell's choice of DSB repair by HR rather than NHEJ. This decision is facilitated by transcription of nascent RNA as an early and pivotal step to promote HR (4,9,19). Furthermore, RNAPII inhibition impairs recruitment of the HR factors recruitment to DSBs at the whole genome level (9).

To address some of the challenging questions in this field, our present study has been designed to assess the hypothesis that unrepaired nucleolar rDNA DSBs are actively moved out to the nucleolar periphery to interact with RNAPII, the latter then promoting the HR repair. In support on this scenario, the inhibition of RNAPII using a specific covalent CDK7 inhibitor, THZ1, which blocks transcription initiation, robustly reduces nucleolar cap formation, and likely shifts the DSB repair pathway choice towards NHEJ. Importantly, impairment of nucleolar cap formation by RNAPII inhibition fuels genome instability and death of human cancer cells.

Results

RNAPII inhibition impairs nucleolar cap formation upon rDNA damage

RNA transcription associated with DNA repair by HR is an essential aspect of accurate DSB repair in nucleoplasm (9). Ribosomal DNA breaks move out to the nucleoli, specifically to the nucleolar caps where HR can repair them with high fidelity, thereby avoiding cis-recombination between rDNA copies to preserve the stability of these vulnerable genomic regions. We hypothesized that inhibition of RNA transcription using RNAPII inhibitors can impair cap formation and, thus, interfere with proper rDNA repair. To address this, we took advantage of our well-characterized human sarcoma U2OS-based cell model that stably expresses the endonuclease Cas9 and a GFP-tagged version of the DNA Damage Response (DDR) protein NBS1 (8) for monitoring cap formation after induction of rDNA DSBs. Briefly, by transfection with guide RNA (gRNA) plasmids targeting rDNA (see table 1) (22), we can induce DSBs specifically in the nucleolus and follow the spatiotemporal kinetics of the ensuing DSB repair (Fig. 1A). The THZ1 compound is an

RNAPII-specific inhibitor, targeting the CDK7 protein kinase, thereby inhibiting Serine-5 phosphorylation (S5P) in the C-terminal domain (CTD) of RNAPII. In our cells, THZ1 treatment efficiently reduced S5P of the RNAPII as revealed by nuclear immunofluorescence intensity upon staining with a RNAPII-S5P antibody (Fig. 1B and C) (20). Inhibition of RNAPII by THZ1 blocks initiation and elongation of nascent RNA transcripts and consequently also reduces DNA end resection as the primary step of the HR-mediated DSB repair (Fig. 1D) (9). The reason why THZ1 treatment also partly reduces DNA resection in cells transfected by an empty vector instead of gRNA reflects the fact that RNAPII also plays a role in repair of endogenous DNA damage (9). Monitoring formation of NBS1-GFP-containing nucleolar caps after transfection of rDNA-specific gRNAs demonstrated that more than 25% of cells accumulated these structures in the nucleolar periphery by 6 hours after gRNA transfection (Fig. 1E and F). Treatment with THZ1 for 2 hours before the 6-hour cap formation assessment time-point (Fig. 1A) revealed an almost 3-fold decrease in the percentage of cells with such rDNA damage-induced cap formation at the nucleolar periphery (Fig. 1E and F). We also confirmed that RNAPII inhibition impaired the number of NSB1-GFP caps formed per cell, consistent with the requirement of RNA transcription activity for efficient cap formation (Fig. 1G). In control experiments, we excluded the possibility that Cas9 levels were affected by RNA transcription inhibition during the 2 hours of treatment with THZ1 (Fig. 1H).

To corroborate the results obtained using stable Cas9 expression in U2OS, we further assayed rDNA DSB behavior in U2OS cells upon transient gRNA transfection and direct transfer of ectopic recombinant Cas9 protein, thereby avoiding the plasmid integration events and potential off-target effects due to stable Cas9 maintenance in the cells. Nucleolar cap formation using this transient expression approach was faster compared with the plasmid-based expression system (7). Indeed, these cells showed nucleolar cap formation already during the first 3 hours after gRNA/Cas9 transfection (Fig. S1A). THZ1 treatment immediately after transfection reduced nucleolar cap formation at 1 hour after transfection and even more robustly, up to 4-fold, after 3 hours of THZ1 exposure. This approach excludes any possible negative impact of either Cas9 or NBS1-GFP stable expression during THZ1 treatment (Fig. S1B), which might affect to S5P of the RNAPII CTD (Fig. S1C).

The decrease of active initiation of RNA transcription upon THZ1 treatment is accompanied by a defective DNA end resection as the primary step of the HR-mediated DSB repair (Fig. 1D), consistent with the dependence of HR repair on nascent RNA synthesis. Taken together, our data suggest that the THZ1 inhibitor impairs nucleolar cap formation, probably due to the requirement of nascent RNA for efficient assembly, and hence function, of the HR machinery at the nucleolar periphery.

Transcription initiation and elongation are essential for accurate rDNA repair

While THZ1 is a potent specific inhibitor of CDK7, hence blocking the initiation of nascent RNA transcript, we asked if other RNAPII inhibitors targeting CDK7, CDK9, CDK12 and CDK13 would also impair cap formation upon induction of rDNA breaks (Fig. 2A). Even a 10-fold lower concentration of THZ1 (0.1 μM), also reduced the percentage of cells with nucleolar caps and number of caps per cells upon Cas9-induced rDNA DSBs (Fig. 2B, C and D). Furthermore, we analysed effects of other RNAPII inhibitors and focused on the next steps of the transcription process. THZ531 is a covalent inhibitor for CDK12/CDK13 when used at low concentrations, 158 and 69 nM, respectively, but it can affect CDK7 and CDK9 at high concentrations (>8.5 μM). THZ531 used at a low concentration (1 μM) had a similar effect to that caused by THZ1 in the NBS1-GFP-Cas9 cells after gRNA-vectors transfection to generate rDNA breaks, followed by a 2-fold decrease of nucleolar caps (Fig. 2B, C and D). This effect suggests that transcription elongation due to the lack of Serine-2 phosphorylation (S2P) of RNAPII CTD caused by CDK12/13 kinase inhibition is also essential for nucleolar cap formation in cells with rDNA DSBs (Fig. 2B, C and D). However, we noticed that THZ531 at this concentration also decreased S5P of the RNAPII CTD domain, similarly to THZ1 (Fig. 2E), suggesting that mainly initiation and, possibly, elongation steps of RNA transcription promote cap accumulation. Then, we investigated other CDK9-targeting drugs that operate through different mechanisms. THAL-SNS-032 is a selective CDK9 degrader PROTAC consisting of a CDK-binding SNS-032 ligand linked to a thalidomide derivative that binds the E3 ubiquitin ligase Cereblon (CRBN)(21). NPV-2 is a potent and selective ATP-competitive cyclin-dependent kinase 9 (CDK9) (22) that inhibits RNAPII at low concentration. Treatment with either inhibitor during 2 hours before nucleolar cap assessment upon rDNA DSB induction demonstrated that any RNAPII dysfunction in S5P-CTD caused by CDK9 inhibition impairs rDNA repair associated with both a decreasing percentage of cells with NBS1-marked nucleolar caps, and the number of caps per cells (Fig. 2B, C and D). These data show that CDK9 inhibition causes a deficiency in DNA repair *via* impairment of RNA transcription. Finally, we used DRB, a classic inhibitor of transcription elongation by RNAPII, yet with a broader spectrum of targets than the other inhibitors used above. DRB treatment also resulted in a lower percentage of cells with NBS1-foci and NBS1-cap structures than seen in the control DMSO-treated cells (Fig. 2B, C and D). To minimize the likelihood of any off-target effect of THZ1, we used another known RNAPII inhibitor, triptolide, that affects RNA transcription initiation by RNAPII degradation via proteasome (9,23). We observed similar nucleolar cap formation deficiency after triptolide treatment, demonstrating that the inhibition of transcription initiation by RNAPII indeed leads to nucleolar cap formation (Fig. S2A and B). All the RNAPII inhibitory compounds used in

this study consistently showed that nascent RNA transcription by RNAPII is essential for cap formation during assembly of HR factors to repair rDNA DSBs.

RNAPII colocalises with nucleolar caps upon rDNA DSB formation.

Recent studies showed that transcription initiation promotes HR factors recruitment at DNA DSBs (4,9,24,25). To further study the relevance of the RNAPII function for nucleolar cap formation upon DSBs in rDNA, we next wondered if the transcription complexes are recruited actively in these DNA repair structures. We took advantage of high-resolution fluorescence imaging of NBS1-GFP-Cas9 U2OS cells after 6 hours post gRNA transfection to induce DSBs in rDNA. First, cells were co-stained with antibodies to transcription initiation markers such as S5P residue in the CTD domain of the RNPII (RNAPII-S5P). As shown in Fig. 3A, the RNAPII-S5P staining is pan-nuclear but reveals accumulation in distinct foci close to the nucleolar periphery. To determine the presence of the transcription initiation complex in the nucleolar caps, we measured the profile dynamics of the DSBs in rDNA visualized by NBS1-GFP and the RNAPII-S5P transcription initiation marker. We observed RNAPII-S5P recruitment to nucleolar caps, significantly colocalising with NBS1, suggesting that active nascent transcription in these regions is spatially coordinated with rDNA repair (Fig. 3A and B). Under these conditions, we also detected a later stage of RNA nascent process using S2P of the CTD domains that drives transcription elongation (RNAPII-S2P). RNAPII-S2P remained localised at the nucleolar caps, although it showed a diffuse colocalisation pattern in some of them (Fig. 3C and D). These results suggest that early transcription steps do occur in the vicinity of the rDNA DSBs at the periphery of the nucleolus, consistent with a functional link between active RNAPII with rDNA repair by HR (9). Finally, we analysed the profile for other phosphorylations in the CTD of the RNAPII, specifically in Tyrosine 1 (RNAPII-Y1P), which some studies have related it to DSB repair (26). Our colocalisation analysis showed that RNAPII-Y1P occupancy in the nucleolar caps was limited to the periphery of the rDNA DSB-containing regions marked by NBS1-GFP (Fig. 3E and F), suggesting that this modification *per se* is unlikely to be directly required for the rDNA repair, despite it is locally connected with the area of RNA-coupled rDNA repair. Taken together, these results suggest a relationship between nascent RNA transcription by RNAPII and nucleolar restructuring for an accurate rDNA repair.

RNAPIII has recently been associated with promoting HR of DSBs, similarly to RNAPII. Therefore, we analysed whether RNAPIII is also present in nucleolar caps as RNAPII, using immunofluorescence (Fig. S3A). Interestingly, the subunit of RNAPIII, RPC32, does not colocalise completely with NBS1-GFP in the nucleolar caps, but partial colocalisation was detected in around nucleolar caps (Fig. S3A and B). Curiously, a subset of nucleolar caps showed a very robust match between NBS1 and RPC32 proteins (Fig. S3C and D), while other nucleolar caps lacked RPC32

entirely, even in the same cell (Fig. S3C and E). These results suggest that both RNAPII and RNAPIII are related to promoting HR in the nucleolar caps, with RNAPII representing a critical, ubiquitously present complex, and RNAPIII likely providing a more context-dependent role in this process.

RNAPII inhibition impairs HR factor recruitment to nucleolar caps.

The movement of rDNA from the nucleolar interior to anchoring points at the periphery is thought to render rDNA breaks accessible to repair factors that are excluded from nucleoli (15). To further understand this process, we next wonder if DNA resection upon rDNA DSB induction by CRISPR occurs in nucleolar caps. Fig. 4A shows native BrdU detection, a marker colocalising with NBS1-GFP after 6 hours of gRNA vector transfection. Immunostaining for native BrdU incorporation is feasible due to the resected 5' DNA strand being accessible as a single stranded DNA (ssDNA) intermediate in the HR repair mechanism (9). Profile analysis showed colocalisation peaks for the NBS1-GFP and BrdU staining, showing an active DNA resection process inside the analysed nucleolar caps (Fig. 4B). To investigate whether this phenomenon depends on nascent RNA transcription, we carried out Proximity Ligation Assay (PLA) to assess recruitment of CtIP and MRE11, as key HR factors for DNA resection machinery forming the CtIP-MRN complex. Immunofluorescence analysis using antibodies against CtIP and NBS1 showed that treatment with the RNAPII inhibitor, THZ1, after rDNA DSB induction in the NBS1-GFP reporter cells reduced the average of PLA spots to half and lowered the percentage of PLA foci per cell (Fig. 4C). The use of RNAPII inhibitor did not alter the CtIP protein level in cells, thereby excluding the possible overall CtIP deficiency under these conditions (Fig. S4). A similar pattern was found for MRE11, a partner protein of NBS1 in the MRN complex involved in the early steps of DNA repair. Whereas MRE11-NBS1 PLA colocalization index increased after Cas9-induced DSBs in rDNA (27) , the inhibition of transcription initiation by THZ1 reduced the interaction between these two factors in the nucleolar caps (Fig. 4D). This decrease is undoubtedly due to the requirement of RNAPII active into the nucleolar cap to repair breaks properly by HR pathway. In order to validate the activity of RNAPII within the nucleolar caps, we conducted an analysis of nascent RNA incorporation using EU. This analysis provided evidence that RNA transcription is necessary for the formation of repair nucleolar caps, as indicated by the colocalization pick of nascent RNA with DNA repair factors such as NBS1 (Fig. 4E). Treatment with THZ1 prevented the formation of nucleolar caps, indicating that RNA plays a crucial role in recruiting the DNA repair machinery, not only within the nuclear context but also within the ribosomal chromatin context.

Ribosomal biogenesis in cells exposed to RNAPII inhibition and rDNA damage.

We demonstrated that RNAPII inhibition and rDNA DSBs generated by CRISPR technology resulted in impaired rDNA damage repair. We therefore wondered whether the treatment with the specific inhibitor of RNAPII might have negatively affected ribosome biogenesis and whether such potential effect would be enhanced upon generation of rDNA DSBs in our model system. Due to the fact that pre-rDNA levels remain stable during the 6-hour experiment after rDNA DSB induction, and ribosome profiling was not affected at 6 hours after gRNA transfection (Fig. S5D-left), we wanted to analyze any potential consequences of such rDNA made also at 24 hours post rDNA DNA damage induction. To this end, we first analysed pre-rRNA processing in U2OS cells by assessing the levels of pre- and mature rRNAs by northern blotting (Fig. S5A). As shown in Fig. S5B and C, inhibition of RNAPII significantly affected pre-rRNA processing assessed by Northern blotting. Thus, upon a treatment for 24 h with THZ1, an accumulation of early (e.g. 47S/45S pre-rRNAs) and later (e.g. 30S, 32S, 12S pre-rRNAs) pre-rRNAs was observed (Fig. S5B and C). In contrast, steady-state levels of mature 18S and 28S rRNAs remained unaffected upon the treatment, likely reflecting the stable nature of ribosomes. The significance of these pre-rRNA processing alterations is unclear, however, it could be related to the limitation of levels of specific protein assembly factors and/or their function following RNAPII inhibition. Importantly, CRISPR-induced rDNA DSBs did neither impede pre-rRNA transcription nor enhanced the observed pre-rRNA processing defects seen after RNAPII inhibition, indicating that this type of rDNA damage did not limit the overall number of actively transcribed rDNA copies. We also studied ribosome biogenesis and function after RNAPII transcription inhibition before and after inducing rDNA DSBs, by polysome profile analysis. As shown in Fig. S5D-right, inhibition of RNAPII transcription by THZ1 led to an alteration in the polysome profiles; while control cells showed a typical peak distribution of free 40S and 60S r-subunits, 80S ribosomes and actively translating polysomes, the THZ1-treated cells showed an increase of the 80S peak and a robust reduction of polysomes. These profiles likely reflect a depletion of mRNAs after the treatment with the RNAPII inhibitor. As for pre-rRNA processing, CRISPR-induced rDNA DSBs on their own did neither lead to any apparent translation defect, and it did not exacerbate those changes observed upon the THZ1 treatment. These results indicated that, *per se*, the rDNA damage induced in our model system does not cause any unspecific or undesirable defects of ribosome biogenesis and function that could influence our results and interpretations (see Discussion).

RNAPII inhibition provokes rDNA instability and cell death in cancer cells.

To assess the biological longer-term consequences of rDNA damage and RNAPII inhibition, we first examined cell survival by clonogenic assay after rDNA damage and THZ1 treatment. Induction

of rDNA DSBs resulted in a robust 3-fold reduction of cell viability (Fig. 5A), consistent with previous work (28). Furthermore, THZ1 treatment sensitized the undamaged cells, and we observed an increased, albeit not synergistic effect on reducing viability when combining rDNA damage induction with RNAPII inhibition (Fig. 5A and S6A). An MTT assay based on the reduction of the tetrazolium salt MTT to a dark-coloured formazan product by metabolically active cells was also performed to complement the cell viability assay results. As previously observed, damage in rDNA alone reduced (2-fold) cell survival (Fig. 5B). Likewise, RNAPII inhibition by THZ1 showed a negative impact on cell viability of both rDNA-damaged and undamaged cells, with a tendency for an additive effect when rDNA damage and THZ1 treatment were combined (Fig. 5B). Results were similar but more pronounced after 24 hours of THZ1 treatment (Fig. S6B)

It is known that nuclear DNA damage can cause mitochondrial dysfunction, and changes in mitochondrial membrane potential may undermine cell viability though apoptosis (29). Thus, we analysed mitochondrial membrane potential after THZ1 treatment for 2 hours in rDNA-damaged and undamaged cells, but no significant differences were observed (Fig. S6C and D). There was a modest, non-significant decrease in membrane potential in cells treated with THZ1 for 24 hours (Fig. S6E). As THZ1 impairs nucleolar cap formation, and defective DNA repair usually leads to an increase in genomic instability. We next investigated whether RNAPII inhibition after rDNA DSB induction may impact genome stability. For this purpose, we analysed micronuclei formation frequency, one of the indicators of genome instability due to DNA damage (30). After rDNA DSB induction, a 2-fold increase of micronuclei formation was observed (Fig. 5C), further enhanced by RNAPII inhibition upon THZ1 treatment (Fig. 5C and D). Notably, rDNA regions were present in the formed micronuclei after rDNA lesion induction and transcription inhibition conditions (Fig. 5D). After 24 hours of THZ1 treatment, results were similar (Fig. S6F). Altogether, our results emphasise the importance of rDNA repair under genotoxic nucleolar stress and highlight the important role of RNAPII in the maintenance of nucleolar homeostasis and rDNA stability.

Discussion

The nucleolus is a potential Achilles' heel of cancer cells. The highly dynamic nucleolar structure, multi-copy repetitive rDNA sequences, and high metabolism rate associated with ribosome biosynthesis mark the rDNA genes as one of the hotspot regions of genomic instability (31). Consequently, rDNA mutations and chromosomal aberrations are more frequent in cancer cells due to their aberrant growth and metabolism, including enhanced protein synthesis (32). In addition, rDNA lesions generated upon oncogenic or genotoxic stresses require special processing to be repaired (8). Genotoxic nucleolar stress evokes rDNA DSB movement to the nucleolar periphery with the ensuing cap formation, to which rapid and efficient recruitment of the HR repair machinery

is required to avoid illegitimate recombination with other repetitive rDNA sequences inside the nucleolus (8). To date, it has not been established what does mechanistically drive the process of relocating the rDNA breaks to nucleolar periphery and the cap formation to facilitate repair of rDNA DSBs by HR.

Our previous study showed that RNAPII is actively recruited to DNA DSBs to promote HR-mediated repair (9). Hence, we hypothesised that rDNA breaks are incorporated to nucleolar caps where RNAPII is active and can direct the DSB repair pathway choice towards the more accurate HR mechanism (see graphical abstract). We took advantage of our recently reported Cas9 system for inflicting DSBs selectively in rDNA regions, generating genotoxic nucleolar stress (33). The data presented in our current study show that RNAPII inhibition by any of several commonly used inhibitors, including THZ1 or DRB, impairs the dynamics of nucleolar cap formation (Fig. 1 and 2), reducing the local accumulation of the NBS1 protein, the leading factor involved in HR-mediated repair of rDNA breaks. Considering that NBS1 is part of MRN (MRE11-RAD50-NBS1), the protein complex that serves as a sensor of DSBs and an essential factor in the DNA end resection (27), our results suggest that RNAPII is involved in the assembly phase as well as the early function of the HR machinery for repair of rDNA DSBs, analogous to DSB processing in other non rDNA genomic regions (9,24,34). We report that RNAPII colocalizes with NBS1 in the nucleolar caps upon rDNA DSB induction, at the same time showing the RNAPII CTD domain phosphorylations on Ser-5 and Ser-2 that represent functional markers of RNAPII-mediated transcription initiation and elongation activities, respectively. Overall we demonstrate that nascent transcription is intimately linked with rDNA breaks under repair in the nucleolar caps. RNAPII-Y1P modification, functionally linked to other aspects of RNAPII activity (35), was not tightly colocalise with nucleolar caps, again consistent with the need for RNAPII-mediated transcription initiation in the early stages of DSB repair by HR.

Interestingly, the 53BP1 protein is also situated at regions of the nucleolar caps. Indeed, Burger *et al.* have suggested a link between this NHEJ factor and Y1P of the RNAPII CTD (26). These data are also consistent with the general role of the RNAPII in promoting HR (9,19,24), regardless of the genomic region affected by the DSB lesions. Notably, RNAPIII is also involved in HR activation in a mode similar to RNAPII (*3*), except that RNAPIII is only present in subsets of nucleolar caps in our expriments, suggesting that its function may be more context-dependent. The initial steps in DNA end resection to shift DSB repair towards HR require CtIP recruitment (10,13,36), as the main partner of MRE11 (37,38), with the role complementary to nascent RNA transcription in DSB processing (9). Our findings support this model, as the recruitment of both MRE11 and CtIP to the nucleolar caps was impaired by THZ1 treatment in cells harbouring rDNA breaks.

It was surprising to find that the overall ribosomal biogenesis pathway was not impacted by rDNA damage within the first 6 to 24 hours, even after the silencing that it is expected for RNAPI (17) . This reflects how strong and viable is the protein synthesis process in cancer cells. However, inhibiting RNAPII resulted in an expected significant depletion of mRNA, leading to the accumulation of monosomes and loss of polysomes. Relevant to cell fate and potential pathological impact of perturbing rDNA repair, we expected to find genome instability in our models of rDNA induction upon RNAPII inhibition, broadly consistent with the postulated propensity of the rDNA regions towards instability under diverse stress conditions (11). Indeed, our present findings using RNAPII inhibitors confirm and further extend those earlier studies (*10*), demonstrating that unrepaired rDNA triggers genome instability by micronuclei formation, including the presence of rDNA regions in these aberrant structures (Fig. 5). Other studies suggested that RNAPII inhibition may increase chromosomal oncogene fusions by alteration of the chromatin distribution (39). Given the strong relationship between genome instability and cancer (11,40,41), our current results also suggest a potential mechanism through which RNAPII inhibition might be exploited in cancer treatment (42), particularly in cancer cells that suffer nucleolar stress, at the same time sensitizing such tumors to treatment by transcriptional inhibitors such as THZ1, which is currently under evaluation in clinical trials (Fig. 5).

In summary, this reports broaden the role of the major RNA polymerase, RNAPII, in the spatio-temporal organisation of the DNA damage response, here under genotoxic nucleolar stress, with implications for better understanding of cell (patho)physiology.

Materials and Methods

Cell culture

U2O-Cas9-NBS1-GFP cells (33) were cultured in Dulbecco's Modified Eagle Medium (DMEM) with high glucose plus GlutaMax supplemented with 10% fetal bovine serum (FBS; Biowest), 100 U/ml penicillin and 100 µg/ml streptomycin (Biowest) at 37 °C in 5% CO_2. U2O-Cas9-NBS1-GFP stably transfected cells were maintained by adding 1 µg/ml puromycin and 0.5 mg/ml neomycin G418 to the medium. Cells were cultured in the presence of different inhibitors (Table 1) using concentrations mentioned in each figure.

Plasmids and transfections

For rDNA DSB induction by CRISPR/Cas9, four guide RNAs (gRNA) plasmids were used (43). Three of them were pMA plasmids expressing sequences targeting rDNA present on all five

acrocentric short arms (Table 2) and the other was a control plasmid expressing the gRNA scaffold but no target sequence. Plasmids carry out ampicillin resistant marker.

Transient transfection of U2OS-Cas9-NBS1-GFP cells was carried out using Lipofectamine LTX with plus reagent (Invitrogen) following manufacturer's instructions. Briefly, cells were seeded in different plate formats, accordingly to the requirements of each specific experiment, to be 70-90% confluent at transfection. Then, the three gRNA plasmids pooled in a ratio 1:1:1 and PLUS reagent were diluted in Opti-MEM and mixed with Lipofectamine LTX Reagent blended into Opti-MEM, in a 1:1 ratio. Solution was incubated 5 min at room temperature and finally was added dropwise to the plate with gentle rocking. Cells were then collected 0-6 hours after transfection unless otherwise indicated.

Inmunofluorescence

Cells were grown on sterile coverslips, transfected with gRNAs as previously described and treated or not with inhibitors as indicated in each figure. Cells were fixed with 4% paraformaldehyde (w/v) in PBS for 10 min, washed twice with PBS and then permeabilised with 0.2% Triton X-100 in PBS for 5 min. Following two washes with PBS, cells were blocked for at least 1 hour with 5% FBS diluted in PBS, incubated with adequate primary antibodies (Table 3) diluted in 5% FBS in PBS for 2 hours at room temperature, washed again with PBS and then, incubated with the appropriate secondary antibodies (Table 3) and 4′-6-diamidino-2-phenylindole (DAPI, 10 ng/ml) in blocking buffer for 1 hour at room temperature in the dark. Coverslips were mounted with Fluoromount-G mounting medium (Invitrogen), and images were acquired using a LEICA microscope. Image analysis was performed by measuring the intensity profile using the IMAGEJ software drawing a line ROI over the image and using the "Plot Profile" tool to generate a graph of intensity values along that line. At least 1000 cells per sample were scored. Experiments were repeated at least three times independently.

High-content image acquisition

Quantitative image-based cytometry (QIBC) was performed as previously described (9). Briefly, the images were acquired in an automatic and unbiased way by scanR acquisition software 3.0 and analysed by scanR image analysis software 3.0. The results were exported as txt files. The txt data set was further processed with spotfire and PRISM 8 software (Graphpad Software Inc) for further analysis. Statistical significance was determined with Ordinary one-way and two-way ANOVA tests using multiple comparisons using PRISM 8 software (Graphpad Software Inc). Statistically significant differences were labelled with one, two, or three asterisks if $p< 0.05$, $p< 0.01$ or $p < 0.001$, respectively.

Metabolic labeling of nascent RNA by EU

Nascent RNA was visualized using metabolic labeling using Invitrogen™ Click-iT™ RNA Alexa Fluor™ 594 imaging kit, with modifications. Briefly, U2OS-Cas9-NBS1-GFP cells were seeded onto coverslips, transfected with gRNAs as previously described, treated 2 hours with 1 μM of THZ1 inhibitor 4 hours after transfection and pulsed for 30 min with EU at a final concentration of 1 mM. Following treatments, cells were fixed with 4% paraformaldehyde (PFA) for 10 min, permeabilised with 0.5% Triton X-100 and washed 3 times with Tris buffered saline (TBS) (50 mM Tris pH 8.0, 150 mM NaCl). Then, samples were incubated 30 min with fresh prepared Click-iT reaction cocktail, containing 5 μM Alexa Fluor 594 azide, 2 mM CuSO4, 100 mM sodium ascorbate. After removal of the reaction cocktail, cells were washed three times with TBS and stained with DAPI. Finally, coverslips were mounted onto glass slides using Fluoromount-G (Invitrogen) and cells were imaged by fluorescence microscopy. Image analysis was performed by measuring the intensity profile using the IMAGEJ software drawing a line ROI over the image and using the "Plot Profile" tool to generate a graph of intensity values along that line.

Immunoblotting

Whole-cell extracts were prepared in Laemmli buffer 2X (4% SDS, 20 % glycerol, 125 mM Tris−HCl, pH 6.8, 0.02% bromophenol blue, 200 mM DTT) by boiling at 100 °C for 10 min and sonicated in a Bioruptor for 2 cycles of 30 sec ON/30 sec OFF at high intensity. Proteins were resolved by SDS-PAGE and transferred to nitrocellulose membranes (AmershamTM Protran® 0.45 µm, GE Healthcare Chicago, IL, USA). Membranes were blocked for 1 hour with 5% BSA in TTBS (15 mM Tris-HCl, pH 7.5, 200 mM NaCl, 0.2 M NaCl, 0.1% (v/v) Tween-20), followed by incubation with the appropriate primary antibodies overnight at 4°C (Table 3). After being washed with TTBS, membranes were incubated with HRP-conjugated secondary antibodies (Table 3) for 1 hour at room temperature. Chemiluminescence was performed using Clarity Western ECL Substrate (Bio-Rad), and results were acquired using the ChemiDoc Touch Imaging System (Bio-Rad) and visualised with Image Lab software 5.1 (Bio-Rad).

Micronuclei assay

Cells were seeded onto coverslips, transfected with gRNAs as previously described and treated 2 hours with 1 μM of THZ1 inhibitor 4 hours after transfection. Following treatment, the medium was replaced by fresh one and cytochalasin B (Sigma) was added at 4 µg/ml. 20 hours post-treatment, cells were fixed in PBS-4% paraformaldehyde 10 min, permeabilised in PBS-0.2%

Triton X-100 5 min, blocked 30 min in blocking buffer (PBS-5% FBS) and incubated 1-2 hours with nucleolin primary antibody (Table 3) in blocking buffer. Cells were then washed two times with PBS and incubated for 45 min with the corresponding secondary antibody (Table 3) diluted in blocking buffer plus DAPI (Sigma) in darkness. Finally, coverslips were washed twice with PBS, dried and mounted onto glass slides using Fluoromount-G (Invitrogen). Micronuclei containing or not nucleolin were counted only from binucleated cells.

Clonogenic survival assay

For clonogenic survival assays, cells were transfected with gRNA as previously described for rDNA DSBs induction and 4 hours post-transfection cells were treated with different concentration (0.1 μM, 0.5 μM, 1μM) of THZ1 or vehicle (DMSO) as control for 2 hours. Then, cells were counted and re-seeded in 6-well plates at two different concentrations, 1000 and 500 cells per well, in triplicates. Cells were then grown at 37º C for 7-8 days to allow colonies formation. Afterwards, plates were washed in PBS and fixed and visualised by staining with 1% methylene blue diluted in 20% ethanol, followed by washes with water to remove the excess of staining. Plates were left to dry overnight and the number of colonies per well was scored for each condition and normalised to the untreated condition.

MTT assay

MTT [3-(4,5-dimethylthiazol-2-yl)-2,5-diphenyltetrazolium bromide] assay (Roche) was performed following manufacturer's indications. After transfection with gRNA and incubation with different concentration (0.1 μM, 0.5 μM, 1 μM) of THZ1 or DMSO for 2 hours as previously described, cells were seeded at a density of 2×10^3 cells/well in 100 μl of medium on a 96-well plate in triplicates. After 5 days growing, 10 μl of MTT (5 mg/ml) was added to each well, and plates were incubated at 37°C for 4 hours. Then, 100 μl of 10% SDS was added, and cells were incubated overnight at 37°C to dissolve the insoluble purple formazan products. A_{570} was measured using a microplate reader with a reference wavelength of 690 nm.

PLA assay

Proximity ligation assay (PLA) was performed using the Duolink In Situ Red Starter Kit Mouse/Rabbit (Sigma-Aldrich) according to the manufacturer's instructions. First, U2OS-Cas9-NBS1-GFP cells were processed like immunofluorescence, blocked with blocking solution from the Duolink PLA Kit for 30 min at 37 °C and staining with specific primary antibodies (Table 3) overnight at 4° C. After that, cells were incubated with MINUS and PLUS secondary PLA probes

for 1 h at 37 °C, and the detection of these probes was carried out using the ScanR microscope (Olympus). The number of PLA signals per nucleus was scored in at least 100 cells per sample.

References

1. Zisi, A., Bartek, J. and Lindstrom, M.S. (2022) Targeting Ribosome Biogenesis in Cancer: Lessons Learned and Way Forward. *Cancers (Basel)*, **14**.
2. Derenzini, M., Trere, D., Pession, A., Montanaro, L., Sirri, V. and Ochs, R.L. (1998) Nucleolar function and size in cancer cells. *Am J Pathol*, **152**, 1291-1297.
3. Weeks, S.E., Metge, B.J. and Samant, R.S. (2019) The nucleolus: a central response hub for the stressors that drive cancer progression. *Cell Mol Life Sci*, **76**, 4511-4524.
4. Liu, S., Hua, Y., Wang, J., Li, L., Yuan, J., Zhang, B., Wang, Z., Ji, J. and Kong, D. (2021) RNA polymerase III is required for the repair of DNA double-strand breaks by homologous recombination. *Cell*, **184**, 1314-1329 e1310.
5. Hilton, J., Gelmon, K., Bedard, P.L., Tu, D., Xu, H., Tinker, A.V., Goodwin, R., Laurie, S.A., Jonker, D., Hansen, A.R. *et al.* (2022) Results of the phase I CCTG IND.231 trial of CX-5461 in patients with advanced solid tumors enriched for DNA-repair deficiencies. *Nat Commun*, **13**, 3607.
6. Lin, Y.L. and Pasero, P. (2012) Interference between DNA replication and transcription as a cause of genomic instability. *Curr Genomics*, **13**, 65-73.
7. Warner, J.R. (1999) The economics of ribosome biosynthesis in yeast. *Trends Biochem Sci*, **24**, 437-440.
8. Korsholm, L.M., Gal, Z., Nieto, B., Quevedo, O., Boukoura, S., Lund, C.C. and Larsen, D.H. (2020) Recent advances in the nucleolar responses to DNA double-strand breaks. *Nucleic Acids Res*, **48**, 9449-9461.
9. Gomez-Cabello, D., Pappas, G., Aguilar-Morante, D., Dinant, C. and Bartek, J. (2022) CtIP-dependent nascent RNA expression flanking DNA breaks guides the choice of DNA repair pathway. *Nat Commun*, **13**, 5303.
10. Gomez-Cabello, D., Jimeno, S., Fernandez-Avila, M.J. and Huertas, P. (2013) New tools to study DNA double-strand break repair pathway choice. *PLoS One*, **8**, e77206.
11. Jackson, S.P. and Bartek, J. (2009) The DNA-damage response in human biology and disease. *Nature*, **461**, 1071-1078.
12. Heyer, W.D., Ehmsen, K.T. and Liu, J. (2010) Regulation of homologous recombination in eukaryotes. *Annu Rev Genet*, **44**, 113-139.
13. Lopez-Saavedra, A., Gomez-Cabello, D., Dominguez-Sanchez, M.S., Mejias-Navarro, F., Fernandez-Avila, M.J., Dinant, C., Martinez-Macias, M.I., Bartek, J. and Huertas, P. (2016) A genome-wide screening uncovers the role of CCAR2 as an antagonist of DNA end resection. *Nat Commun*, **7**, 12364.
14. Larsen, D.H. and Stucki, M. (2016) Nucleolar responses to DNA double-strand breaks. *Nucleic Acids Res*, **44**, 538-544.
15. van Sluis, M. and McStay, B. (2015) A localized nucleolar DNA damage response facilitates recruitment of the homology-directed repair machinery independent of cell cycle stage. *Genes Dev*, **29**, 1151-1163.
16. Kruhlak, M., Crouch, E.E., Orlov, M., Montano, C., Gorski, S.A., Nussenzweig, A., Misteli, T., Phair, R.D. and Casellas, R. (2007) The ATM repair pathway inhibits RNA polymerase I transcription in response to chromosome breaks. *Nature*, **447**, 730-734.
17. Larsen, D.H., Hari, F., Clapperton, J.A., Gwerder, M., Gutsche, K., Altmeyer, M., Jungmichel, S., Toledo, L.I., Fink, D., Rask, M.B. *et al.* (2014) The NBS1-Treacle complex controls ribosomal RNA transcription in response to DNA damage. *Nat Cell Biol*, **16**, 792-803.

18. Lesage, E., Clouaire, T. and Legube, G. (2021) Repair of DNA double-strand breaks in RNAPI- and RNAPII-transcribed loci. *DNA Repair (Amst)*, **104**, 103139.
19. Domingo-Prim, J., Endara-Coll, M., Bonath, F., Jimeno, S., Prados-Carvajal, R., Friedlander, M.R., Huertas, P. and Visa, N. (2019) EXOSC10 is required for RPA assembly and controlled DNA end resection at DNA double-strand breaks. *Nat Commun*, **10**, 2135.
20. Nilson, K.A., Guo, J., Turek, M.E., Brogie, J.E., Delaney, E., Luse, D.S. and Price, D.H. (2015) THZ1 Reveals Roles for Cdk7 in Co-transcriptional Capping and Pausing. *Mol Cell*, **59**, 576-587.
21. Olson, C.M., Jiang, B., Erb, M.A., Liang, Y., Doctor, Z.M., Zhang, Z., Zhang, T., Kwiatkowski, N., Boukhali, M., Green, J.L. *et al.* (2018) Pharmacological perturbation of CDK9 using selective CDK9 inhibition or degradation. *Nat Chem Biol*, **14**, 163-170.
22. Aoi, Y., Takahashi, Y.H., Shah, A.P., Iwanaszko, M., Rendleman, E.J., Khan, N.H., Cho, B.K., Goo, Y.A., Ganesan, S., Kelleher, N.L. *et al.* (2021) SPT5 stabilization of promoter-proximal RNA polymerase II. *Mol Cell*, **81**, 4413-4424 e4415.
23. Wang, Y., Lu, J.J., He, L. and Yu, Q. (2011) Triptolide (TPL) inhibits global transcription by inducing proteasome-dependent degradation of RNA polymerase II (Pol II). *PLoS One*, **6**, e23993.
24. Vitor, A.C., Sridhara, S.C., Sabino, J.C., Afonso, A.I., Grosso, A.R., Martin, R.M. and de Almeida, S.F. (2019) Single-molecule imaging of transcription at damaged chromatin. *Sci Adv*, **5**, eaau1249.
25. Meisenberg, C., Pinder, S.I., Hopkins, S.R., Wooller, S.K., Benstead-Hume, G., Pearl, F.M.G., Jeggo, P.A. and Downs, J.A. (2019) Repression of Transcription at DNA Breaks Requires Cohesin throughout Interphase and Prevents Genome Instability. *Mol Cell*, **73**, 212-223 e217.
26. Burger, K., Schlackow, M. and Gullerova, M. (2019) Tyrosine kinase c-Abl couples RNA polymerase II transcription to DNA double-strand breaks. *Nucleic Acids Res*, **47**, 3467-3484.
27. Chapman, J.R. and Jackson, S.P. (2008) Phospho-dependent interactions between NBS1 and MDC1 mediate chromatin retention of the MRN complex at sites of DNA damage. *EMBO Rep*, **9**, 795-801.
28. Warmerdam, D.O., van den Berg, J. and Medema, R.H. (2016) Breaks in the 45S rDNA Lead to Recombination-Mediated Loss of Repeats. *Cell Rep*, **14**, 2519-2527.
29. Wang, K., Gong, Q., Zhan, Y., Chen, B., Yin, T., Lu, Y., Zhang, Y., Wang, H., Ke, J., Du, B. *et al.* (2019) Blockage of Autophagic Flux and Induction of Mitochondria Fragmentation by Paroxetine Hydrochloride in Lung Cancer Cells Promotes Apoptosis via the ROS-MAPK Pathway. *Front Cell Dev Biol*, **7**, 397.
30. Hatch, E.M., Fischer, A.H., Deerinck, T.J. and Hetzer, M.W. (2013) Catastrophic nuclear envelope collapse in cancer cell micronuclei. *Cell*, **154**, 47-60.
31. Salim, D. and Gerton, J.L. (2019) Ribosomal DNA instability and genome adaptability. *Chromosome Res*, **27**, 73-87.
32. Lindstrom, M.S., Jurada, D., Bursac, S., Orsolic, I., Bartek, J. and Volarevic, S. (2018) Nucleolus as an emerging hub in maintenance of genome stability and cancer pathogenesis. *Oncogene*, **37**, 2351-2366.
33. Korsholm, L.M., Gal, Z., Lin, L., Quevedo, O., Ahmad, D.A., Dulina, E., Luo, Y., Bartek, J. and Larsen, D.H. (2019) Double-strand breaks in ribosomal RNA genes activate a distinct signaling and chromatin response to facilitate nucleolar restructuring and repair. *Nucleic Acids Res*, **47**, 8019-8035.
34. Jimeno, S., Prados-Carvajal, R. and Huertas, P. (2019) The role of RNA and RNA-related proteins in the regulation of DNA double strand break repair pathway choice. *DNA Repair (Amst)*, **81**, 102662.

35. Mayer, A., Heidemann, M., Lidschreiber, M., Schreieck, A., Sun, M., Hintermair, C., Kremmer, E., Eick, D. and Cramer, P. (2012) CTD tyrosine phosphorylation impairs termination factor recruitment to RNA polymerase II. *Science*, **336**, 1723-1725.
36. Huertas, P. and Jackson, S.P. (2009) Human CtIP mediates cell cycle control of DNA end resection and double strand break repair. *J Biol Chem*, **284**, 9558-9565.
37. Buis, J., Stoneham, T., Spehalski, E. and Ferguson, D.O. (2012) Mre11 regulates CtIP-dependent double-strand break repair by interaction with CDK2. *Nat Struct Mol Biol*, **19**, 246-252.
38. Anand, R., Ranjha, L., Cannavo, E. and Cejka, P. (2016) Phosphorylated CtIP Functions as a Co-factor of the MRE11-RAD50-NBS1 Endonuclease in DNA End Resection. *Mol Cell*.
39. Yasuhara, T., Xing, Y.H., Bauer, N.C., Lee, L., Dong, R., Yadav, T., Soberman, R.J., Rivera, M.N. and Zou, L. (2022) Condensates induced by transcription inhibition localize active chromatin to nucleoli. *Mol Cell*, **82**, 2738-2753 e2736.
40. Lord, C.J. and Ashworth, A. (2012) The DNA damage response and cancer therapy. *Nature*, **481**, 287-294.
41. Streffer, C. (2010) Strong association between cancer and genomic instability. *Radiat Environ Biophys*, **49**, 125-131.
42. Wang, J., Zhang, R., Lin, Z., Zhang, S., Chen, Y., Tang, J., Hong, J., Zhou, X., Zong, Y., Xu, Y. *et al.* (2020) CDK7 inhibitor THZ1 enhances antiPD-1 therapy efficacy via the p38alpha/MYC/PD-L1 signaling in non-small cell lung cancer. *J Hematol Oncol*, **13**, 99.
43. van Sluis, M. and McStay, B. (2017) Nucleolar reorganization in response to rDNA damage. *Curr Opin Cell Biol*, **46**, 81-86.
44. Rodriguez-Hernandez, M.A., Gonzalez, R., de la Rosa, A.J., Gallego, P., Ordonez, R., Navarro-Villaran, E., Contreras, L., Rodriguez-Arribas, M., Gonzalez-Gallego, J., Alamo-Martinez, J.M. *et al.* (2018) Molecular characterization of autophagic and apoptotic signaling induced by sorafenib in liver cancer cells. *J Cell Physiol*, **234**, 692-708.
45. Sloan, K.E., Mattijssen, S., Lebaron, S., Tollervey, D., Pruijn, G.J. and Watkins, N.J. (2013) Both endonucleolytic and exonucleolytic cleavage mediate ITS1 removal during human ribosomal RNA processing. *J Cell Biol*, **200**, 577-588.

Acknowledgments

Thanks to Fernando Gómez Herreros´s lab for helpful discussions. Thanks to Oliver Quevedo for technical advice and discussions.

Funding:

R+D+I PID2022-137280OB-I00. Ministry of Science and Innovation
AECC-Investigator Grant (INVES20017GOME)
University of Seville-Plan Propio-Grant: 2021/00001263 (PV, GS)
MSCA-IF-2017 (795930)
R+D+i PID2019-103850-GB-I00 (MCIN/AEI/10.13039/501100011033.
Andalusian Regional Government (P20_00581, BIO-271)
University of Seville (US-1380394, US/JUNTA/FEDER,UE).
Novo Nordisk Foundation (NNF20OC0060590)
Danish Council for Independent Research (DFF-7016-00313)
Swedish Research Council (VR-MH 2014-46602-117891-30)
Danish National Research Foundation (project CARD, DNRF 125)
Danish Cancer Society (R204-A12617-B153)

Author contributions:

Conceptualisation: DGC, JB
Methodology: CCR, BSQ, OQ, LC, DGC

Investigation: JCD, JB, DGC
Supervision: DGC
Writing—original draft: DGC
Writing—review & editing: CCR, JCD, JB, DGC

Competing interests: The authors declare no competing interests.

Data and materials availability: All data, code, and materials used in the analyses must be available in some form to any researcher for purposes of reproducing or extending the analyses.

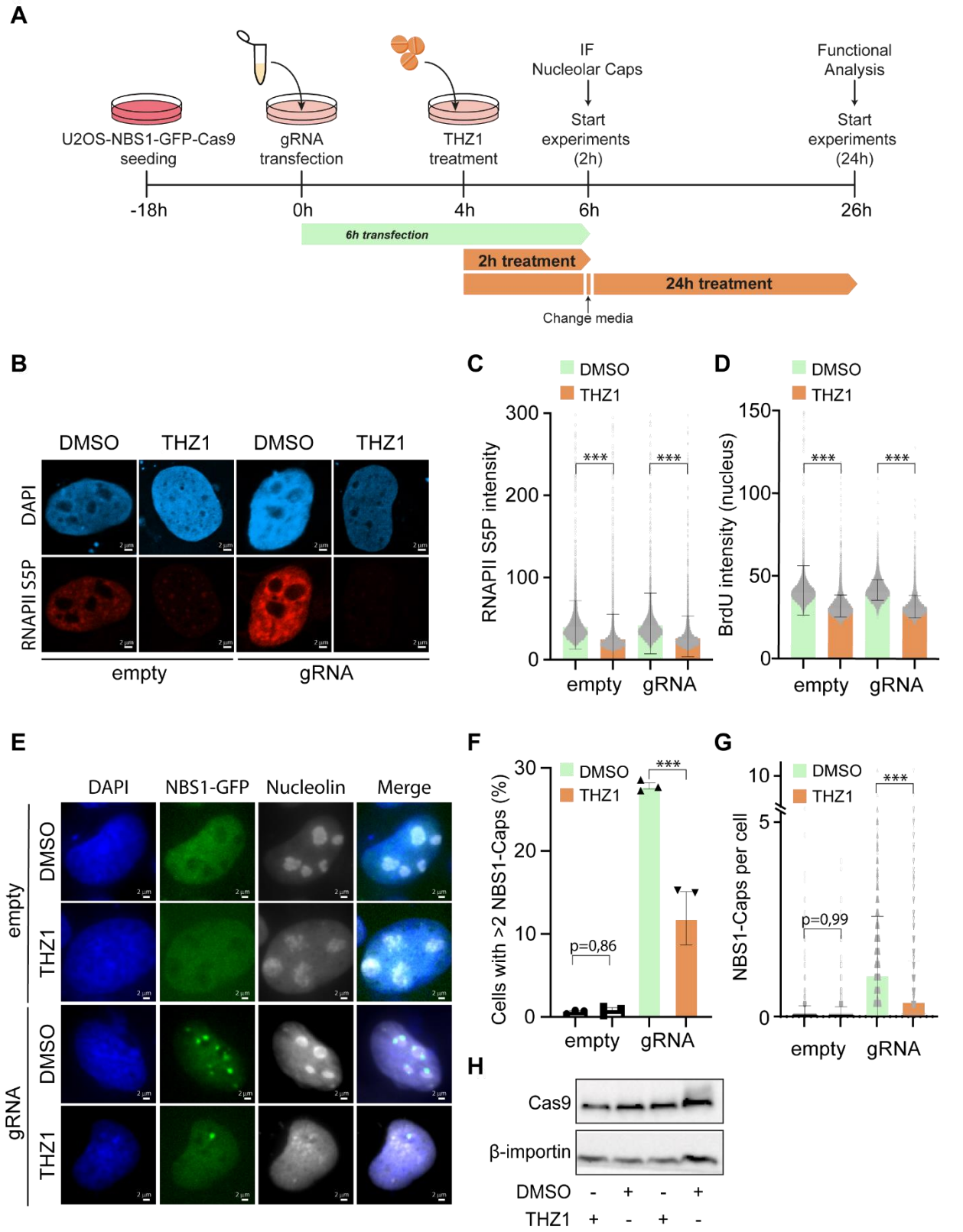

Fig. 1. Checca-Rodríguez, et al.

Fig. 1. RNAPII inhibition results in impaired nucleolar caps formation. (**A**) Schematic illustration of the experimental timeline. U2OS-NBS1-GFP-Cas9 cells were seeded at the start of

experiments. The following day, cells were transfected with gRNA targeting rDNA or the control empty vector for 6 hours (green box). 4 hours post-transfection cells were treated with THZ1 for 2 or 24 hours (orange box). In the case of 24h-treatment, media was replaced after 2 hours to eliminate the transfection agents and THZ1 was added again in the fresh medium. Finally, cells were collected and differently processed depending on the experiment. (**B**) Representative fluorescence microscopy images of RNAPII phosphorylated in Serine-5 (RNAPII-S5P; red) after gRNA transfection and THZ1 treatment. Nuclei were stained with DAPI. Scale bar: 2 μm. (**C**) Quantification of RNAPII S5P intensity in cells from (B). A representative experiment from 3 replica is shown. At least 1000 cells were quantified. (**D**) Quantification of BrdU staining under non-denaturing conditions to mark ssDNA as a DNA resection marker in the same conditions as in (B). (**E**) Representative microscopy images of nucleolar caps marked with NBS1-GFP in U2OS-NBS1-GFP-Cas9 following rDNA DSBs induction by gRNA transfection and RNAPII inhibition by THZ1 treatment. Nuclei were stained with DAPI and nucleoli with anti-nucleolin antibody. Scale bar: 2 μm. (**F**) The percentage of cells with more than two nucleolar caps upon DSBs induction and RNAPII inhibition is plotted. Graph represents the average and SEM of 3 independent experiments. At least 1000 cells were count. (**G**) Number of nucleolar caps per cell in the same conditions as in (F). A representative experiment of 3 is shown. (**H**) Cas9 levels analysed by western blotting from whole protein extract of U2OS-NBS1-GFP-Cas9 cells transfected with gRNA and treated with THZ1. β-importin was used as a loading control. Statistical significance was calculated with Ordinary One-way Anova (* $p<0.05$; ** $p<0.01$; *** $p<0.001$).

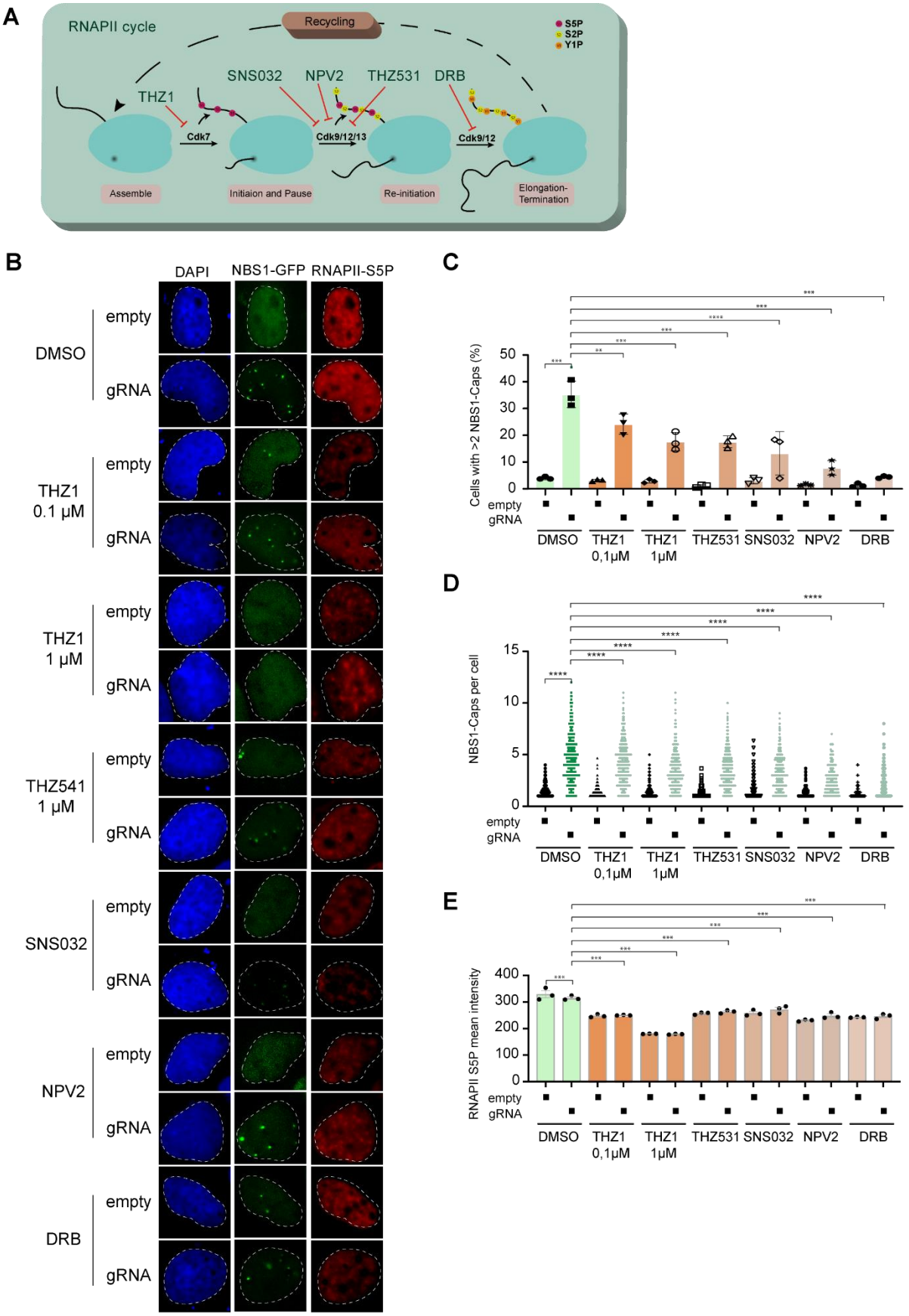

Fig. 2. Checa-Rodríguez, et al.

Fig. 2. RNAPII transcription initiation and elongation are essential to accurate rDNA repair. (**A**) Representative image of RNAPII transcription cycle for showing assembly, initiation and pause, re-initiation and elongation-termination stages. Phosphorylation of different residues are marked: Serine-5 phosphorylation (red circles), Serine-2 phosphorylation (yellow circles) and Tyrosine 1 phosphorylation (orange circles). Different RNAPII inhibitors with their targets are shown (**B**) Representative fluorescence images of NBS1-GFP nucleolar caps (green) and RNAPII S5P (red) of U2OS-NBS1-GFP-Cas9 cells transfected with the gRNA or the empty control and treated with the different RNAPII inhibitors indicated. (**C**) Percentage of cells in the conditions of (B) with more than two nucleolar caps. Graph represents the average and SEM of 3 independent experiments. At least 1000 cells were count**.** (**D**) Number of nucleolar caps per cell in the same conditions as in (B). A representative experiment of 3 replicas is shown. (**E**) Graph shows nuclear quantification of RNAPII S5P intensity under the experimental conditions cued in (B). At least 1000 cells were quantified. The average and SEM of 3 experiments is shown. Statistical significance was calculated with Ordinary One-way Anova (* $p<0.05$; ** $p<0.01$; *** $p<0.001$).

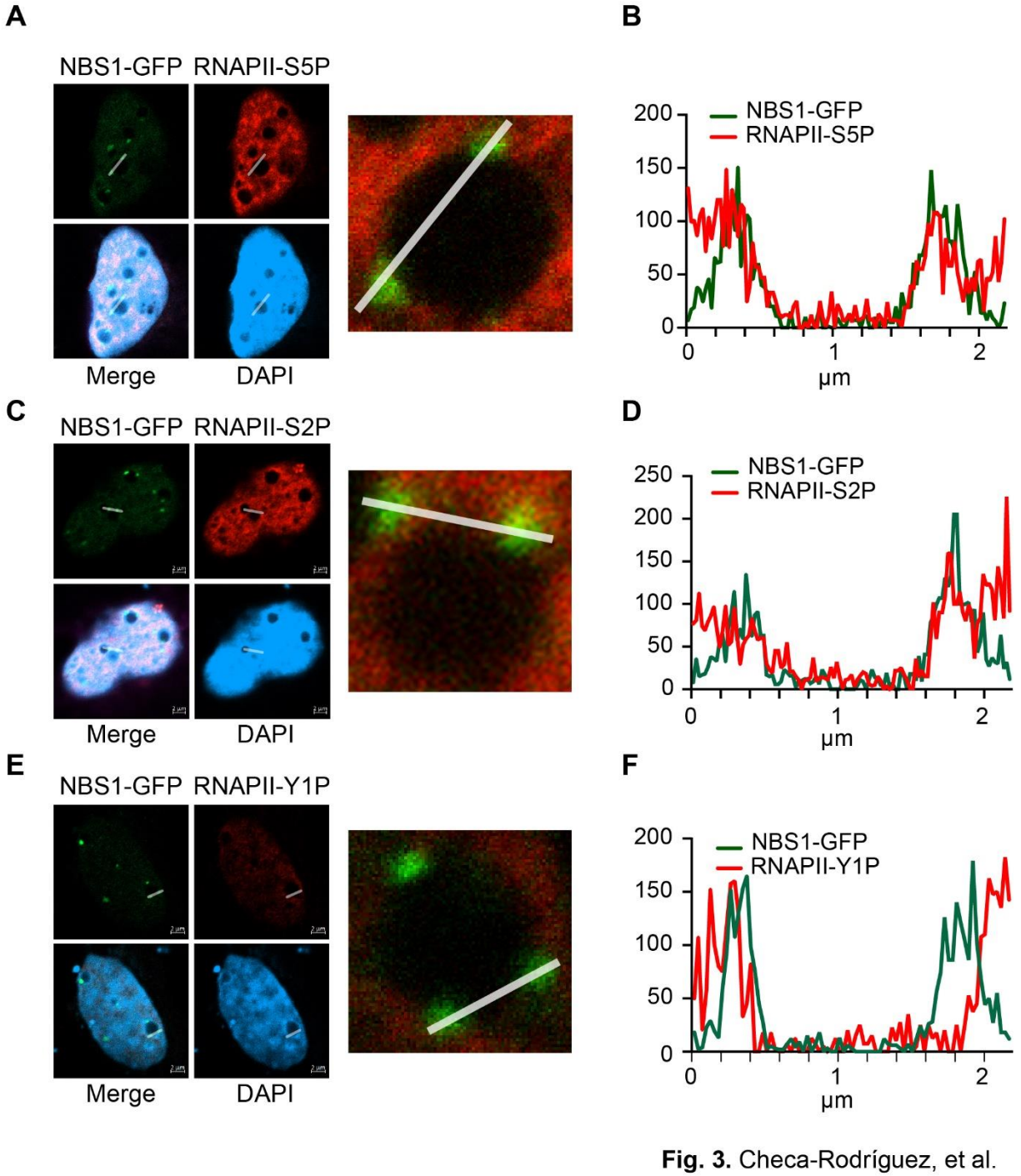

Fig. 3. RNAPII colocalises with nucleolar caps. (**A**) Representative fluorescence images for NBS1-GFP (green) and RNAPII-S5P (red) fluorescence from U2OS-NBS1-GFP-Cas9 cells transfected with gRNA to induce rDNA DSBs. Right zoomed images show in detail the position of line scanned for fluorescent intensity measurement. Scale bar: 2 µm. (**B**) Representative intensity profile for NBS1-GFP and RNAPII-S5P fluorescence across the line shown in (A). At least 10 images of 3 biologically independent experiments were quantified. (**C**) Same as (A) but for RNAPII-S2P (red). (**D**) Same as (B) for RNAPII-S2P. (**E**) Same as (A) but for RNAPII-Y1P (red). (**F**) Same as (B) for RNAPII-Y1P.

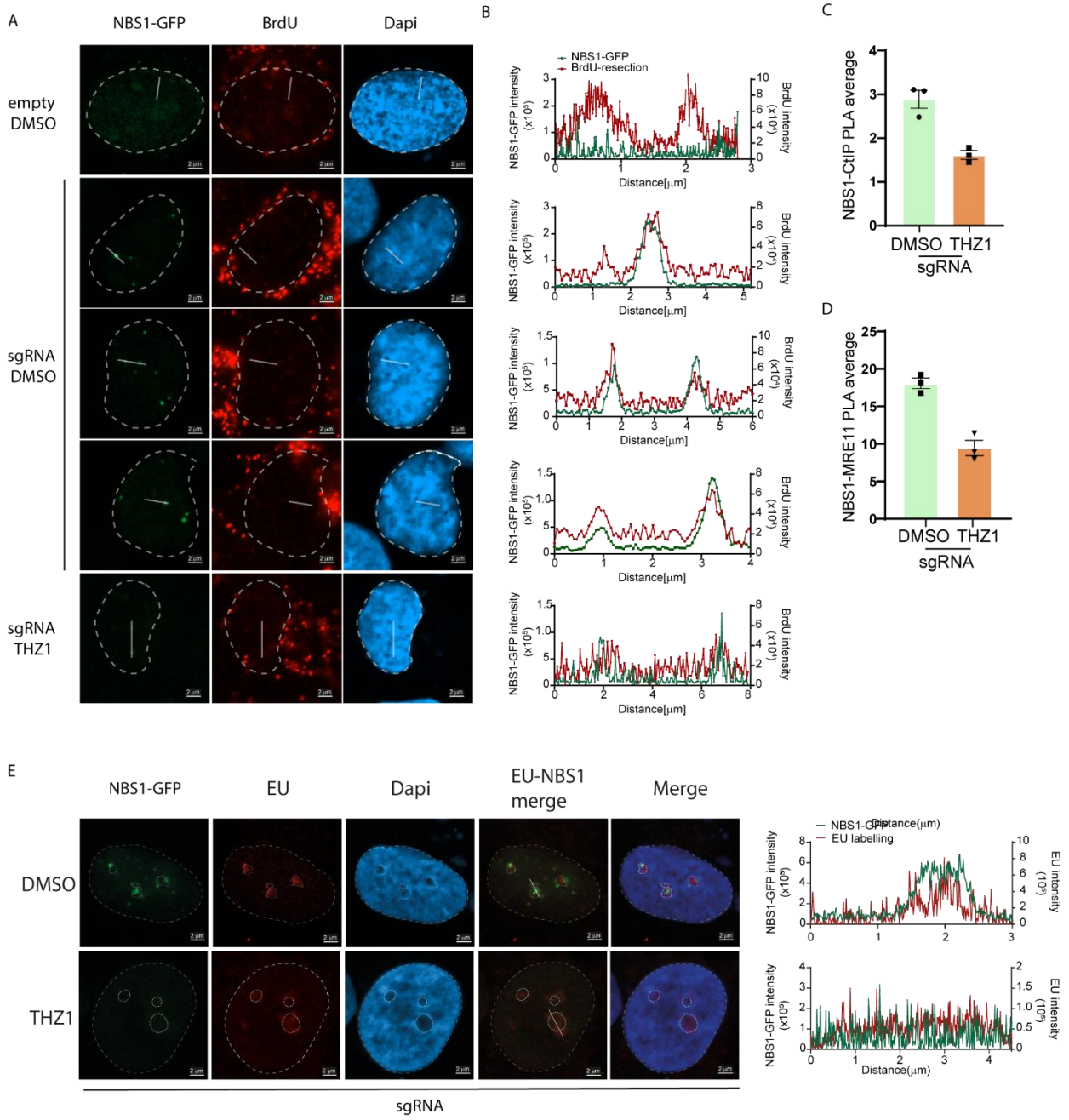

Fig. 4. DNA resection is affected by RNAPII inhibitor in the nucleolar cap. (**A**) Representative fluorescence images of NBS1-GFP (green) and BrdU (red) colocalisation upon gRNA transfection, THZ1 treatment and under non-denaturing conditions. Scale bar: 2 μm. (**B**) Representative fluorescence intensity profiles for NBS1-GFP (green) and BrdU (red) quantified along the traced line in (A). At least 10 images of 3 biologically independent experiments were quantified. (**C**) Graph shows the average number of NBS1-CtIP PLA foci (Proximity ligation assay) for protein interactions among NBS1 and CtIP after gRNA transfection and THZ1 treatment. At least 1000 cells of 3 independent experiments were analysed. (**D**) Same than (C) for average number of NBS1-MRE11 PLA foci per cell. At least 1000 cells of 3 independent experiments were analysed. Statistical significance was calculated with unpaired t test (* $p<0.05$; ** $p<0.01$; *** $p<0.001$). (**E**) Representative immunofluorescence images of NBS1-GFP (green), EU (red) and DAPI (blue) in

U2OS-Cas9-NBS1-GFP upon gRNA transfection, THZ1 treatment and 30-minute labeling with EU. Scale bar: 2 µm. (**F**) Representative fluorescence intensity profiles for NBS1-GFP (green) and EU (red) quantified along the traced line in (E). At least 10 images of 3 biologically independent experiments were quantified.

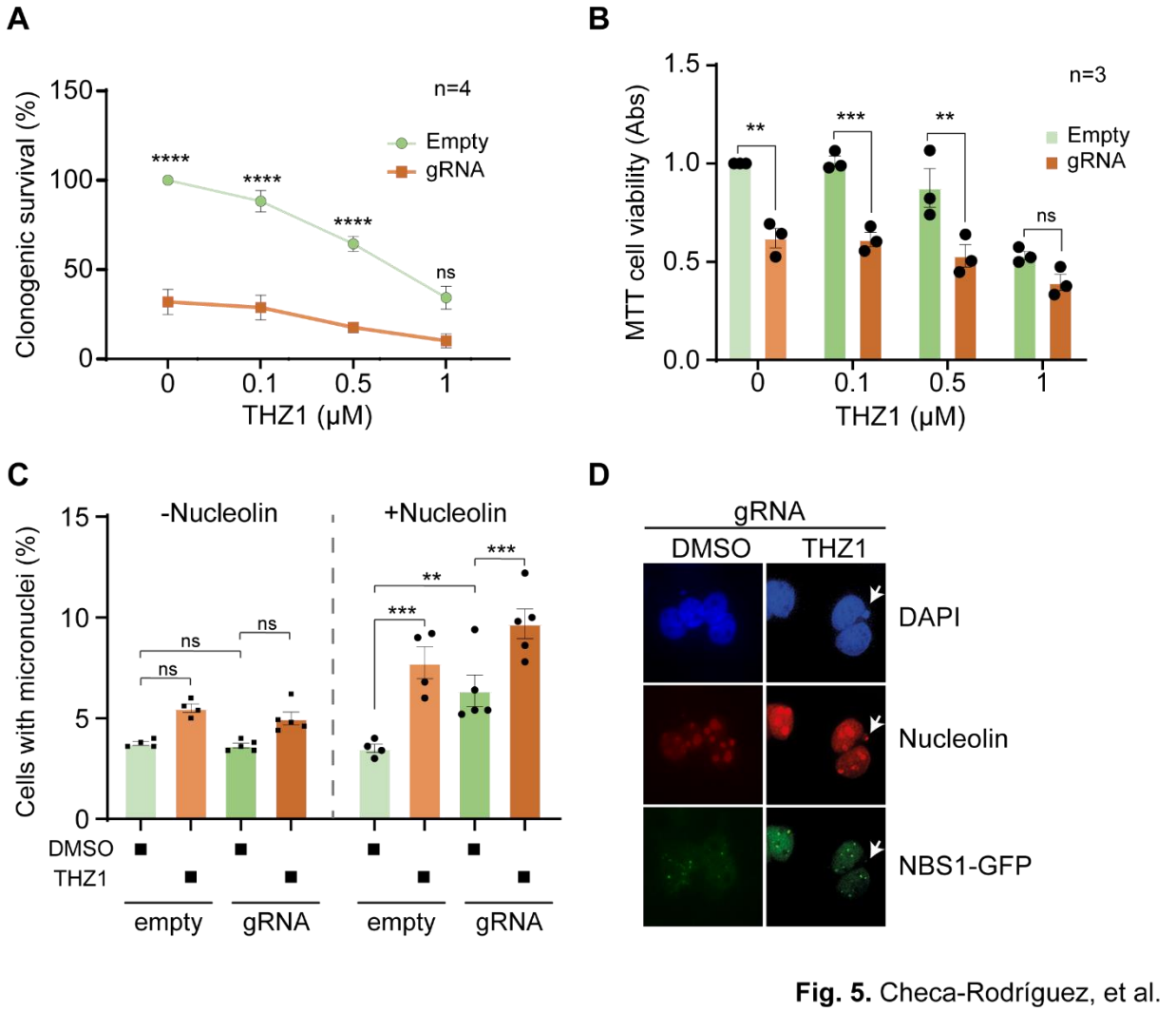

Fig. 5. Checa-Rodríguez, et al.

Fig. 5. RNAPII inhibition affects cell viability and rDNA stability. (**A**) Percentage of clonogenic cell survival of U2OS-NBS1-GFP-Cas9 cells following rDNA DSBs induction and THZ1 treatment compared with the undamaged and untreated control (Empty – DMSO). Cells were transfected with a vector expressing a guide RNA targeting the rDNA (gRNA) or an empty vector as a control (Empty) and treated with different concentrations (0.1 µM, 0.5 µM, 1 µM) of THZ1 or DMSO as control for 2 hours. 7-8 days later, clones were stained with methylene blue. In each experiment, the average number of colonies per condition was scored in triplicates. The average and SEM of four independent experiments are plotted. (**B**) Cell viability measured by MTT assay upon transfection and THZ1 treatment as in (A) and after 5 days of growing following MTT treatment. Graph represents the mean and SEM of 3 independent experiments performed with technical

triplicates, relative to undamaged and untreated control. (**C**) Percentage of cells with micronuclei containing or not nucleolin, after gRNA transfection and 2 hours of 1 μM THZ1 treatment. Micronuclei was scored in 500 binucleated U2OS-NBS1-GFP-Cas9 cells per experiment. The average and SEM of 3 independent experiments is shown. (**D**) Representative fluorescence microscopy images of U2OS-NBS1-GFP-Cas9 cells with micronuclei after DSBs induction and THZ1 treatment. DNA is shown in blue, nucleolin in red and NBS1-GFP in green. An example of micronucleus is indicated by a full white arrow. Statistical significance was calculated with two-way ANOVA (* $p<0.05$; ** $p<0.01$; *** $p<0.001$).

Table 1. sgRNA sequences.

CRISPR vector	Sequence (5´-3´)
rDNA gRNA1	GCGAGAACAGCAGGCCCGC
rDNA gRNA2	GCCTTCTCTAGCGATCTGAG
rDNA gRNA3	GATTTCCAGGGACGGCGCCT

Table 2. RNAPII inhibitors

Drug	Reference	Commercial	Use Concentration	Time of treatment
THZ1	532372	CalbioChem	1 μM	2 hours
THZ531	HY-103618-	MedChemExpress	1 μM	2 hours
NPV2	1702809-17-3	R&D systems	250 nM	3 hours
THAL-SNS032	6532/5	R&D systems	250 nM	3 hours
DRB	D1916	Sigma	100 μM	2 hours
Triptolide	T3652	Sigma	10 μM	30 min

Table 3: Antibodies.

Antibody	Species	Reference / Suppliers	Application
Nucleolin	Rabbit	Abcam; ab70493	IF (1:1000)
Cas9	Mouse	Abcam; ab191468	WB (1:1000)
β-importin	Mouse	Abcam; ab2811	WB (1:5000)
RNAPII pS5	Rabbit	Abcam; ab5131	IF (1:2000)
RNAPII pS2	Rabbit	Abcam; ab5095	IF (1:2000)
RNAPII pY1	Mouse	Active Motif; 61383	IF (1:1000)
BrdU	Rat	Bio-rad AbD Serotec; OBT0030	IF (1:500)
RNAPIII	Mouse	Santa Cruz; SC-48365	IF (1:500)
Mre11	Mouse	Abcam; ab214	IF (1:500)
CtIP	Mouse	Active Motif; 61141	IF/WB (1:500)
HRP-conjugated goat anti-mouse IgG (H+L)	Goat	Jackson, 111-035-146	WB (1:5000)
Alexa Fluor 647 anti-rabbit	Goat	Invitrogen, A21245	IF (1:1000)
Alexa Fluor 546 anti-rabbit	Goat	Invitrogen, A11010	IF (1:1000)
Alexa Fluor 546 anti-mouse	Goat	Invitrogen, A11003	IF (1:1000)

Supplementary Materials

Please use the *Science Advances* template to format your Supplementary Materials.